2

Chapter 2

Heat and Mass Transport for Elastico-Viscous Fluid with Partial Slip Boundary over a Flat Permeable Plate

2.1 Introduction

Elastico-viscous fluid belongs to the class of non-Newtonian fluids exhibiting viscous and elastic properties. During the motion of such type of fluid, elasticity helps to store strain energy in the material while viscosity is responsible for energy dissipation. The application of such fluid is often noticed in chemical, mechanical, and petroleum industries. The technological importance of this fluid draws the attention of many researchers. Extensive research work in this field is going on for the last few decades [31-34].

The transport of heat along with mass in the fluid has lots of applications in science and engineering fields. In nature, it helps in the formation of fog. The thermal and mass diffusion arising from buoyancy forces initiated many transport processes. Examples include catalytic reactors, nuclear reactors, heat exchangers, cooling devices, solar collectors, petroleum resources, metallurgical and chemical resources, etc. Choudhury *et al.* [35] investigated the hydromagnetic visco-elastic fluid flow taking inclined surface and studied the heat and mass transport phenomena with viscous dissipation. Rashidi *et al.* [36]

presented the heat flow for mixed convective hydromagnetic visco-elastic fluid over a permeable wedge. He considered the homotopy method to analyze the thermal radiation effect on the flow field. Hayat *et al.* [37] examined the heat transport for mixed convective elastic-viscous fluid past a stretching cylinder. Nayak *et al.* [38] presented the thermal and mass transport impact on hydromagnetic elastic-viscous fluid past a stretching porous sheet. The viscous and Joule dissipation along with chemical reaction is also taken into account in this study. Farhangmehr *et al.* [39] demonstrated the mechanism of enhancement of heat transition and mass transfer for magnetohydrodynamic nanofluid over a sheet taking nonlinear boundary conditions. The relevant recent studies on heat and mass transport are evident from the literature of the reference papers [40-44].

The dynamics of fluids are triggered from the bounding surface and thus boundary layer fluid flow plays an important role in fluid dynamics. The application of such flow is often observed in engineering and technological processes for the evaluation of drag produced by the friction of bodies in the fluid domain. Blasius [45], firstly studied the progress of velocity in the boundary layer when fluid flows over a flat surface. Pohlhausen [46] investigated the heat transport phenomenon of Blasius result. The numerical investigation of Blasius's findings of flow problems was further carried out by Howarth [47].

The fluid-particle when comes in contact with a solid boundary, is observed in many practical applications that it does not take the velocity of the surface and slips along the surface as it has a fixed tangential velocity. Such a flow is termed as partial slip flow at the boundary. The application of this type of flow is noticed in the chemical industry and in medical treatment. The mixed convective fluid flow past a vertical plate for unsteady case in parallel stream presented by Patil *et al.* [48]. The slip impact on the fluid motion taking pressure and buoyant forces into account over vertical plates investigated by many researchers: Aziz *et al.* [49], Bhattacharyya and Layek [50], Cao and Baker [51], Turkyilmazoglu [52].

The present investigation aims to discuss the heat transition and mass transport mechanism for elastico-viscous fluid flow with slip effects over a flat permeable plate. The study also intended to analyze the impact of different involved flow feature parameters in the velocity, temperature, and concentration profiles. The non-Newtonian fluid model Walters Liquid (Model $B^{'}$) [53-54] is taken for Elastico-viscous fluid. The finite difference method-based solver 'bvp4c' of MATLAB code is employed for the mathematical

computation of governing equations. The computed results are plotted with involved flow parameters for discussion to bring out physics insight into the fluid flow.

2.2 Mathematical Formulation

The incompressible steady laminar elastico-viscous boundary layer slip flow past a flat permeable plate is considered. The transition of heat and mass phenomena are incorporated into the fluid domain by the thermal and concentration equations. Fig. 2.1 depicts the fluid model geometry. Considering boundary layer approximations, the fluid motion is guided by a set of partial differential equations:

$$\frac{\partial \mathrm{u}}{\partial \mathrm{x}} + \frac{\partial \mathrm{v}}{\partial \mathrm{y}} = 0 \tag{2.2.1}$$

$$\mathrm{u}\frac{\partial \mathrm{u}}{\partial \mathrm{x}} + \mathrm{v}\frac{\partial \mathrm{u}}{\partial \mathrm{y}} = \nu\frac{\partial^2 \mathrm{u}}{\partial \mathrm{y}^2} - \frac{\mathrm{k}_0}{\rho}\left[\mathrm{u}\frac{\partial^3 \mathrm{u}}{\partial \mathrm{x}\,\partial \mathrm{y}^2} + \mathrm{v}\frac{\partial^3 \mathrm{u}}{\partial \mathrm{y}^3} - \frac{\partial \mathrm{u}}{\partial \mathrm{y}}\frac{\partial^2 \mathrm{u}}{\partial \mathrm{x}\,\partial \mathrm{y}} - \frac{\partial \mathrm{v}}{\partial \mathrm{y}}\frac{\partial^2 \mathrm{u}}{\partial \mathrm{y}^2}\right] - \frac{\nu}{\mathrm{k}}(u - U_\infty) \tag{2.2.2}$$

$$\mathrm{u}\frac{\partial \mathrm{T}}{\partial \mathrm{x}} + \mathrm{v}\frac{\partial \mathrm{T}}{\partial \mathrm{y}} = \frac{\mathrm{K}}{\rho C_p}\frac{\partial^2 \mathrm{T}}{\partial \mathrm{y}^2} \tag{2.2.3}$$

$$\mathrm{u}\frac{\partial \mathrm{C}}{\partial \mathrm{x}} + \mathrm{v}\frac{\partial \mathrm{C}}{\partial \mathrm{y}} = D_M\frac{\partial^2 \mathrm{C}}{\partial \mathrm{y}^2} + D_T\frac{\partial^2 \mathrm{T}}{\partial \mathrm{y}^2} \tag{2.2.4}$$

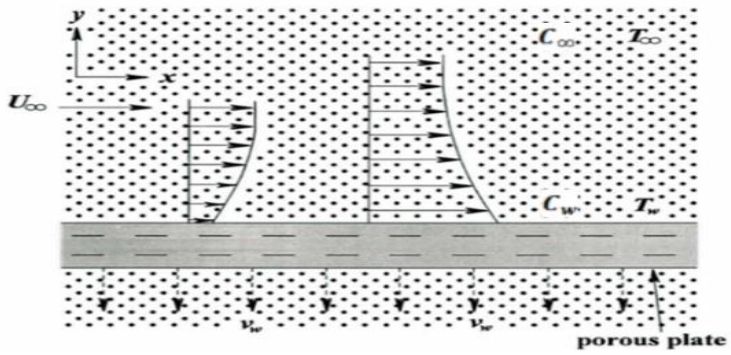

Fig. 2.1 Sketch of fluid model geometry

Imposed conditions at the boundary are:

$$\text{At y} = 0, u = F_1\left(\frac{\partial \mathrm{u}}{\partial \mathrm{y}}\right), v = v_w;\ \text{as}\ y \to \infty,\ u \to U_\infty \tag{2.2.5}$$

$$\text{At y} = 0, T = T_W + G_1\left(\frac{\partial \mathrm{T}}{\partial \mathrm{y}}\right);\ \text{as}\ \ y \to \infty, T \to T_\infty \tag{2.2.6}$$

$$\text{At y} = 0, C = C_W + H_1\left(\frac{\partial \mathrm{C}}{\partial \mathrm{y}}\right);\ \text{as}\ y \to \infty, C \to C_\infty \tag{2.2.7}$$

where, $F_1 = F_0(Re_x)^{\frac{1}{2}}$, $G_1 = G_0(Re_x)^{\frac{1}{2}}$, $H_1 = H_0(Re_x)^{\frac{1}{2}}$, $Re_x = \frac{U_\infty x}{\nu}$, $v_w = \frac{v_0}{(x)^{\frac{1}{2}}}$, $v_0 < 0$: suction, $v_w = \frac{v_0}{(x)^{\frac{1}{2}}}$, $v_0 > 0$: blowing.

To obtain self-similar forms of the above equation, the following similarity transformation is introduced:

$$\Psi = \sqrt{U_\infty \nu x}\, f(\eta), T = T_w + (T_w - T_\infty)\theta(\eta), C = C_w + (C_w - C_\infty)\phi(\eta) \quad (2.2.8)$$

where, $\eta = \frac{y}{x}\sqrt{Re_x}$ and stream function Ψ satisfies $u = \frac{\partial \Psi}{\partial y}$ and $v = -\frac{\partial \Psi}{\partial x}$.

Using relation (2.2.8) in (2.2.2), (2.2.3), and (2.2.4), the following set of self-similar equations are obtained:

$$f'''(\eta) + \tfrac{1}{2} f(\eta) f''(\eta) + k_1 \left[2f'(\eta)f'''(\eta) + \quad f(\eta)f^{iv}(\eta) - \left(f''(\eta)\right)^2\right] +$$

$$k^*\left(1 - f'(\eta)\right) = 0 \quad (2.2.9)$$

$$\theta''(\eta) + \tfrac{1}{2} Pr f(\eta)\theta'(\eta) = 0 \quad (2.2.10)$$

$$\phi''(\eta) + \tfrac{1}{2} S_c f(\eta)\phi'(\eta) + S_c S_r \theta''(\eta) = 0 \quad (2.2.11)$$

where, $k^* = \frac{1}{Da_x Re_x}$, $Da_x = \frac{k}{x^2}$, $Pr = \frac{\mu C_p}{K}$, $S_c = \frac{\nu}{D_M}$, $S_r = \frac{(T_w - T_\infty)D_T}{(C_w - C_\infty)\nu}$.

The boundary conditions (2.2.5), (2.2.6), (2.2.7) transformed as:

$$f(\eta) = S,\ f'(\eta) = \delta f''(\eta)\ at\ \eta = 0\ ;\ f'(\eta) = 1,\ f''(\eta) = 0\ as\ \eta \to \infty \quad (2.2.12)$$

$$\theta(\eta) = 1 + \beta\theta'(\eta)\ at\ \eta = 0\ ; \theta(\eta) = 0\ as\ \eta \to \infty \quad (2.2.13)$$

$$\phi(\eta) = 1 + \gamma\phi'(\eta)\ at\ \eta = 0\ ;\ (\eta) = 0\ as\ \eta \to \infty \quad (2.2.14)$$

where, $S = \left(-\frac{2v_w}{U_\infty}\right)(Re_x)^{\frac{1}{2}} = -\frac{2,v_0}{(U_\infty \nu)^{\frac{1}{2}}}$, $S > 0$ for

$v_0 < 0$ represents suction and $S < 0$ for $v_0 > 0$ represents blowing, $\delta = \frac{F_0 U_\infty}{\nu}$, $\beta = \frac{G_0 U_\infty}{\nu}$ and $\gamma = \frac{H_0 U_\infty}{\nu}$.

2.3 Method of Solution

The numerical method 'bvp4c' of Matlab is a collocation method used to solve the differential equations of the form $\frac{dy}{dx} = \mathrm{g(x, y, q)}$, $\mathrm{x} \in [a, b]$ with non-linear boundary conditions $\mathrm{h(y(a), y(b), q)} = 0$, where vector q is an unknown parameter. This method is an effective solver different from the shooting method and it is based on an algorithm. It can compute inexpensively the approximate value of $y(x)$ for any x in $[a, b]$ taking boundary conditions at every step. In this method, the infinity conditions at the boundary are replaced with a finite point that reasonably satisfies the given problem.

The resultant equations (2.2.9), (2.2.10), and (2.2.11) of fluid motion together with boundary conditions (2.2.12), (2.2.13), and (2.2.14) are computed using the

'bvp4c'MATLAB program code. To implement 'bvp4c', the first-order system is set as follows:

$$f = f_1, f' = f_2,\ f'' = f_3, f''' = f_4\ , \theta = f_5, \theta' = f_6\ , \phi = f_7, \phi' = f_8 \tag{2.3.1}$$

From (2.3.1), we can write

$$f_1' = f_2, f_2' = f_3, f_3' = f_4, f_5' = f_6,\ f_7' = f_8 \tag{2.3.2}$$

Using (2.3.1) and (2.3.2), above equations (2.2.9), (2.2.10), and (2.2.11) can be written as:

$$f_4' = \frac{1}{f_1}\left[(f_3)^2 - 2f_2f_4 - \left(\frac{1}{k_1}\right)\left\{f_4 + \frac{1}{2}f_1f_3 + k^*(1 - f_2)\right\}\right] \tag{2.3.3}$$

$$f_6' = -\frac{1}{2}Prf_1f_6 \tag{2.3.4}$$

$$f_8' = -\frac{1}{2}S_cf_1f_8 - S_cS_rf_6' \tag{2.3.5}$$

and boundary conditions (2.2.11), (2.2.12), and (2.2.13) transformed as:

$$f_1(0) = S, f_2(0) = \delta f_3(0)\ and\ \ f_2(\infty) = 1, f_3(\infty) = 0 \tag{2.3.6}$$

$$f_5(0) = 1 + \beta f_6(0)\ \ and\ \ f_5(\infty) = 0 \tag{2.3.7}$$

$$f_7(0) = 1 + \gamma f_8(0)\ \ and\ \ f_7(\infty) = 0 \tag{2.3.8}$$

2.4 Results and Discussion

To bring out a realistic reason for heat transition and mass transport for elastico-viscous fluid flow over a flat permeable plate with slip effects, the numerically evaluated results are plotted for different values of flow feature parameters involved in the solution viz., elastic-viscous parameter (k_1), permeability parameter (k^*), suction parameter (S), velocity slip parameter (δ), thermal slip parameter (β), mass slip parameter (γ), Prandtl number (Pr), Schmidt number (S_c), Soret number (S_r). While varying one flow parameter to observe the deviation in curves, other involved flow parameters are kept fixed as shown in graphs. The values of flow feature parameters are taken arbitrarily keeping in mind the present problem after going through the reference paper. The boundary conditions at infinity for the velocity, temperature, and concentration profiles are replaced by the number 6 and which appears to justify the conditions as observed from the obtained figures.

To validate the present work and to check the accuracy of numerically obtained results by MATLAB solver 'bvp4c', $f''(0)$ i.e. the skin friction coefficient is evaluated without considering elastico-viscous and permeability parameters. The obtained results are

compared with standard earlier published results and are found in good accord as shown in Table 2.1.

Table 2.1 Comparison of $f''(0)$ for $k_1 = k* = S = \delta$=0

	Howarth [47]	Bhattacharyya and Layek [42]	Present Work
$f''(0)$	0.33206	0.332058	0.3322

The elastico-viscous effects on the velocity profile, temperature profile, and concentration profile are presented in Figs. 2.2, 2.3, and 2.4. Figure 2.2 indicated that the velocity enhances with the growth of elastico-viscous parameter for a while. It is interpreted that thermal motion deforms the polymers of elastico-viscous material and increases the fluid motion. From Fig. 2.3 and 2.4, it is found that the temperature and the mass concentration profiles diminish with the rise of elastico-viscous parameter. As fluid becomes more viscous it hinders the transition of thermal energy to the fluid easily and thus temperature curves decrease. The fluid concentration diminishes because of the temperature drop in the fluid. The movement of the molecules becomes slower and thus collide less and making the fluid less reactive. The more fluid mass deported from the plate towards the fluid domain due to concentration drops.

The impact of permeability factor on the velocity, temperature, and concentration profiles are illustrated from Figs. 2.5, 2.6, and 2.7. With the growth of the permeability parameter, Darcian body force diminishes and thus reduces the fluid motion as noticed in Fig. 2.5. It is observed from Figs. 2.6 and 2.7, that the incremental values of permeability parameter enhance the fluid temperature and the mass concentration. Increasing permeability cause to decrease in the thickness of the momentum boundary layer and thus enhance the temperature of the fluid. As concentration increases with permeability, the mass transfer rate reduces from the fluid towards plate.

The velocity profile, temperature profile, and concentration profile with variation of suction parameter are shown in Figs. 2.8, 2.9, and 2.10. As the fluid particles are absorbed through a porous plate, the fluid motion diminishes and causes a reduction in velocity and momentum boundary layer thickness as noticed in Fig. 8. The increasing values of suction bring fluid near to the plate and diminish the fluid temperature and the mass concentration as observed in Fig. 2.9 and 2.10.

Figures 2.11, 2.12, and 2.13 illustrate the impact of slip parameters on the velocity, temperature, and concentration profiles. The transport of fluid through the porous plate enhances the growth of the velocity slip parameter as noticed in Fig. 2.11. The temperature of the fluid reduces with growing values of the thermal slip parameter as less heat is deported from the porous plate to the fluid as observed from Fig. 2.12. The fluid concentration diminishes with the growth of mass slip parameter as shown in Fig. 2.13. As concentration reduces more mass is transferred from the fluid toward the plate.

Lastly, the concentration profiles are drawn in Figs. 2.14 and 2.15 for incremental values of Schmidt number and Soret number. The growth of the Schmidt number reduces the concentration profile as noticed in Fig. 2.14. The result is justified as mass diffusivity enhances the thickness of the concentration boundary layer due to inverse variation of Schmidt number to mass diffusivity. Figure 2.15 illustrates that with the rise of the Soret number, the concentration profile enhances. The outcome is justified as the concentration boundary layer thickness becomes thick for bigger values of Soret number.

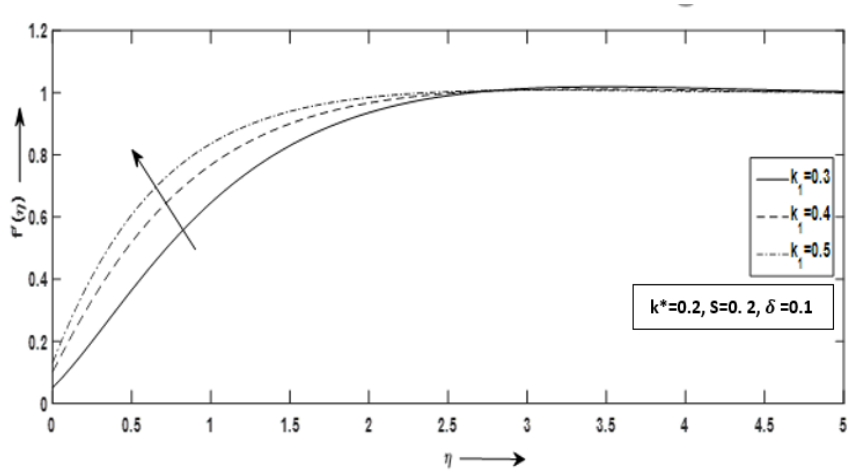

Fig. 2.2 Velocity profile $f'(\eta)$ against η for variation of k_1

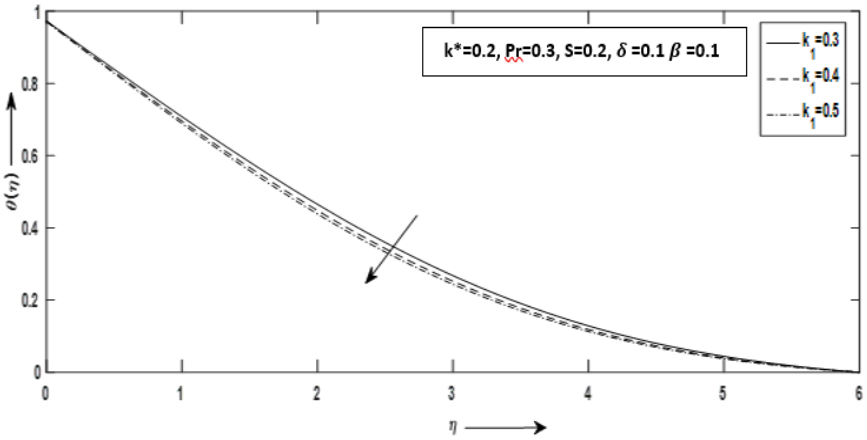

Fig. 2.3 Temperature profile $\theta(\eta)$ against η for variation of k_1

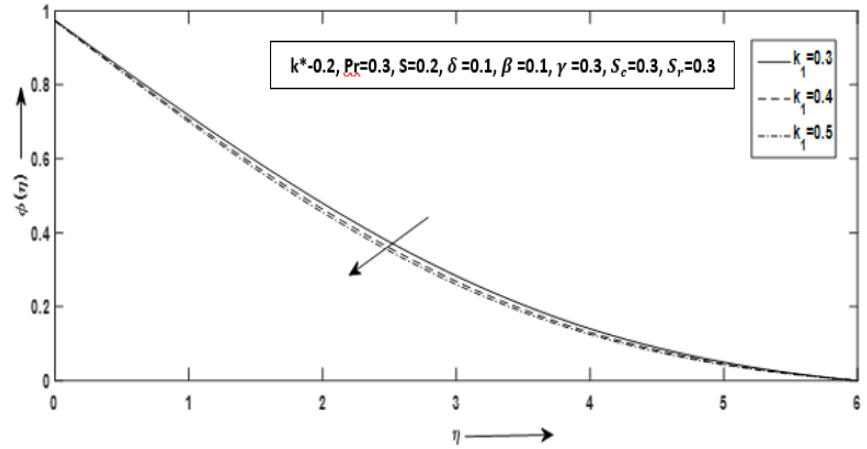

Fig. 2.4 Concentration profile $\phi(\eta)$ against η for variation of k_1

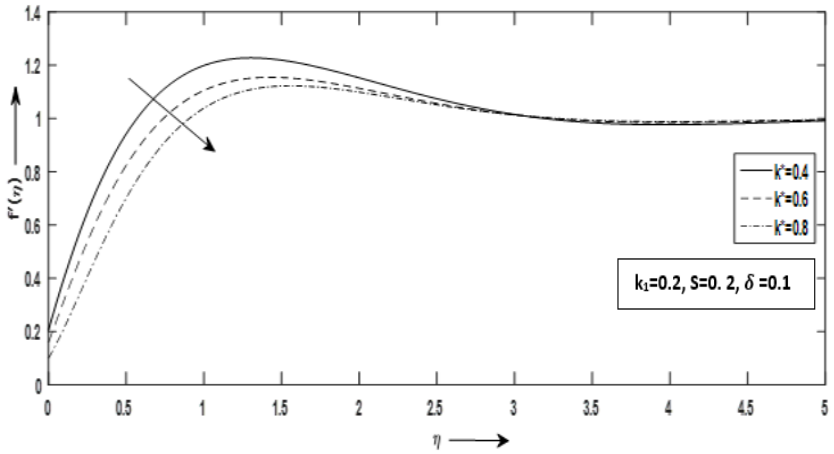

Fig. 2.5 Velocity profile $f'(\eta)$ against η for variation of k*

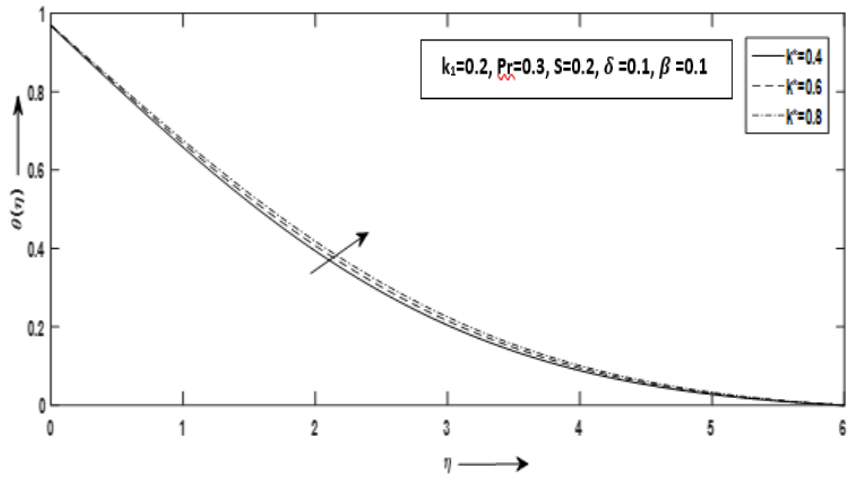

Fig. 2.6 Temperature profile $\theta(\eta)$ against η for k*

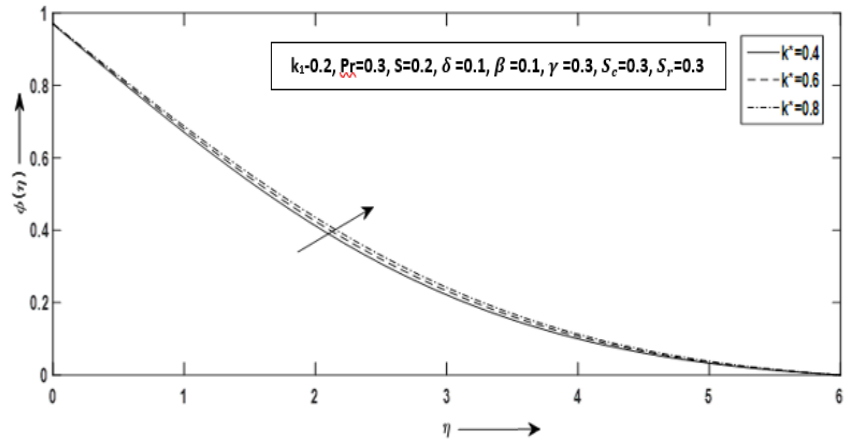

Fig. 2.7 Concentration profile $\phi(\eta)$ against η for variation of k*

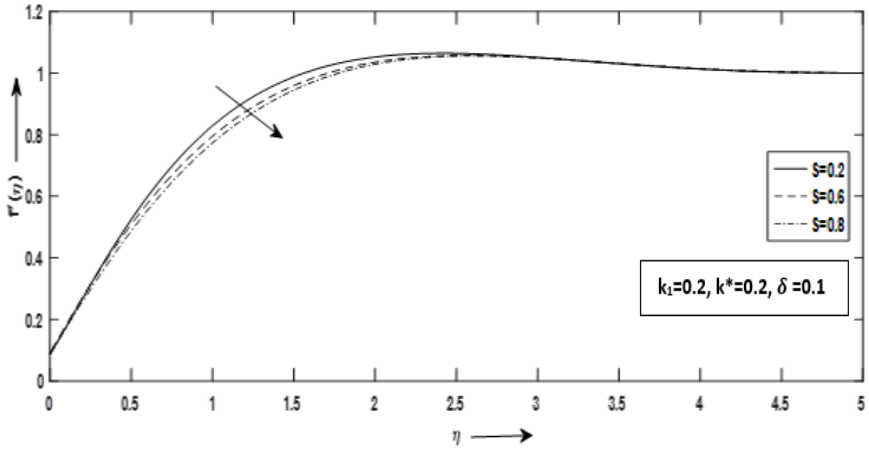

Fig. 2.8 Velocity profile $f'(\eta)$ against η for variation of S

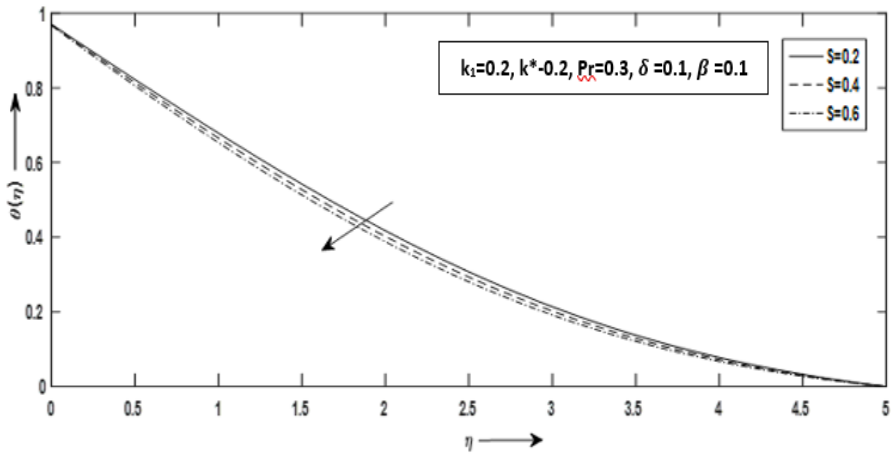

Fig. 2.9 Temperature profile $\theta(\eta)$ against η for variation of S

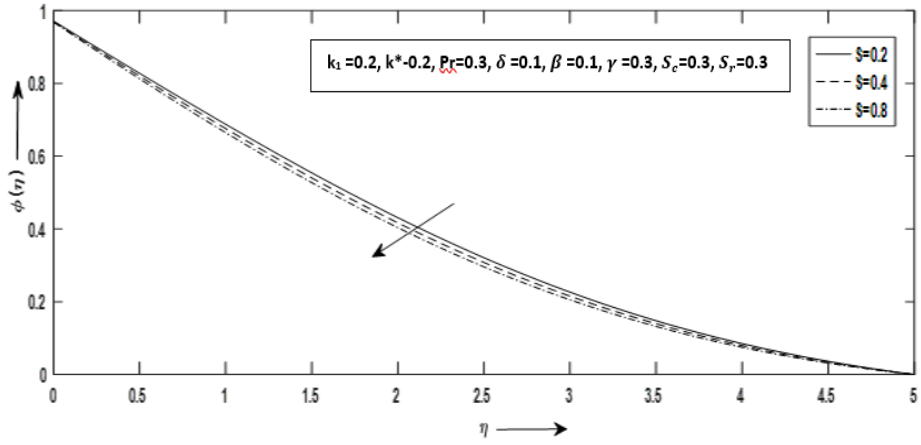

Fig. 2.10 Concentration profile $\phi(\eta)$ against η for variation of S

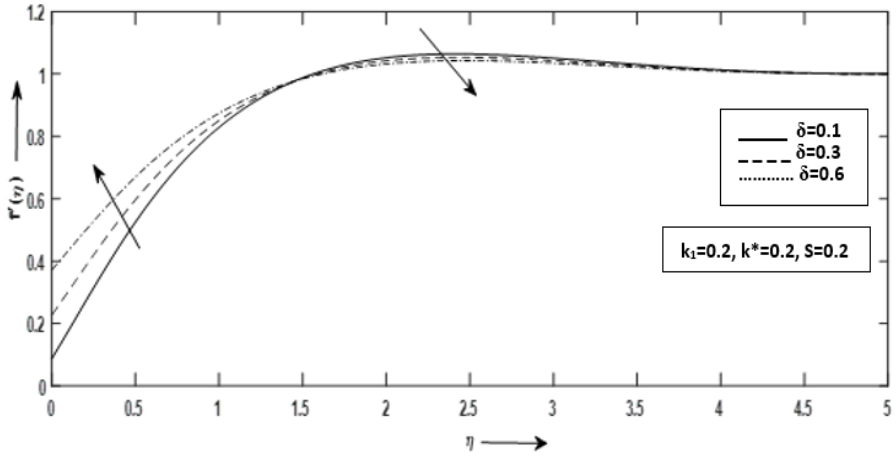

Fig. 2.11 Velocity profile $f'(\eta)$ against η for variation of δ

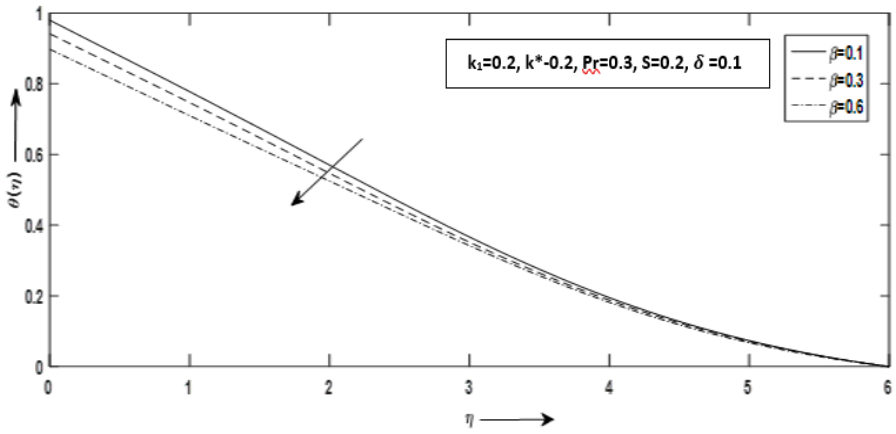

Fig. 2.12 Temperature profile $\theta(\eta)$ against η for variation of β

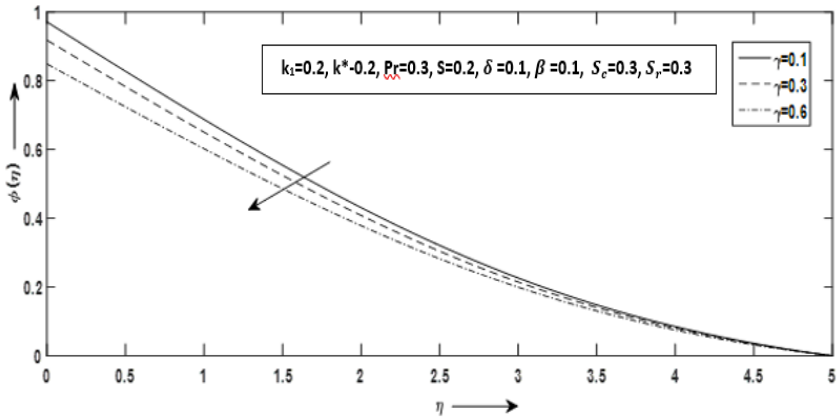

Fig. 2.13 Concentration profile $\phi(\eta)$ against η for variation of γ

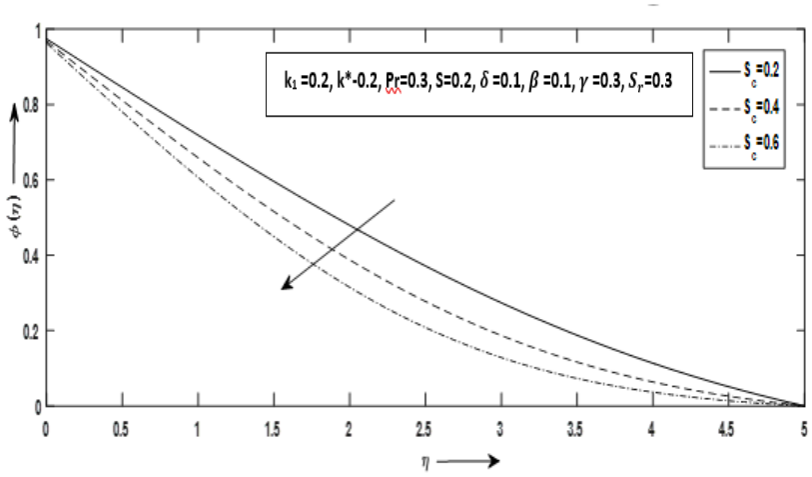

Fig. 2.14 Concentration profile $\phi(\eta)$ against η for variation of S_c

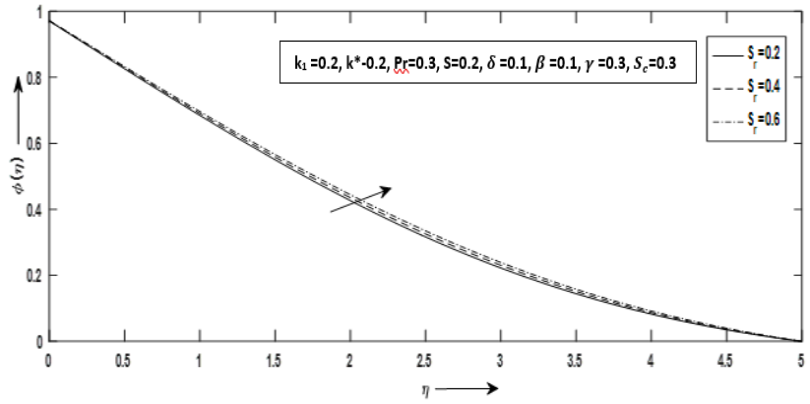

Fig. 2.15 Concentration profile $\phi(\eta)$ against η for variation of S_r

2.5 Conclusions

The study reveals that the heat and mass transport is highly influenced by the elastico-viscous, slip, and other involved flow feature parameters. There is ample scope to extend this work. It may be possible to study the same problem by employing different analytical and numerical methods to compare the obtained results. Flow simulation of the problem may give a clear picture of the obtained results.

The important conclusions are stated below:

- The Transition of thermal energy deforms the molecules of the elastico-viscous fluid and thus velocity reduces even if there is a growth of elastico-viscous parameter.
- As fluid becomes more viscous, temperature drops which help to diminish the concentration of the fluid, and thus more fluid mass is transferred to the flat plate.
- Rising permeability diminishes the Darcian body forces and thus fluid velocity reduces but enhances the fluid temperature and the concentration. The less amount of fluid mass transferred to the plate with the growth of permeability parameter
- As applied suction increases, the velocity, temperature, and concentration reduce, and thus more mass is transferred to the plate.
- As the slip parameter enhances, the fluid velocity increases initially but it drops with distance as suction increases passive resistance but the temperature and concentration of the fluid diminishes and thus helping to increase the mass transport to the plate.

- Increasing the Schmidt number, diminishes the concentration of the fluid, and thus more mass is transferred to the plate. But with the rise of the Soret number, less mass is transferred to the plate.